Revista Brasileira de Física, Vol. 10, Nº 3, 1980

# Mössbauer Studies of Iron Sulphide Minerals

*VIJAYENDRA K. GARG*

*Departamento de Física e Química, Universidade Federal do Espírito Santo, 29000 Vitória, ES, Brasil*

Recebido em 12 de Maio de 1979

## 1. INTRODLICTION

Severa1 of the metal sulphides which occur as minerals have important technological applications because of their electrical and magnetic properties. The use of zinc, lead and cadrnium chalcogenides in photovoltic devices, for example, has resulted in vast literature on the physical properties and electronic structure of these minerals. The technologically valuable electrical and magnetic properties have stimulated, in general, considerable interest in the studies of sulphides for detailed measurements and development of electronic structure models. There are six known minerals of iron sulphide:

1. pyrite ($FeS_2$)
2. marcasite ($FeS_2$)
3. pyrrhotite ($Fe_{1-x}S$, x varies from 0 to 0.125)
4. mackinawite ($FeS_{1-x}$, x varies from 0 to 0.11)
5. greigite ($Fe_3S_4$)
6. smythite ($Fe_3S_4$)

These can be classified into two groups, first showing the simple quadrupole splitting (pyrite and marcasite) and the second showing magnetic hyperfine splitting (pyrrhotite), macknawite, greigite and smythite). Here we will consider the minerals of the first group only.

X.Ray investigations, and investigations of their magnetic and electrical properties[1-6] for both pyrite and marcasite, indicate iron to be in $2^+$ state. There have been conflicting reports[7-9] as to whether $FeS_2$ is

paramagnetic or diamagnetic. Montano & Seehra[10] made a Mössbauer study of pyrite in an external magnetic field up to 35.8 koe at 4.2K, fig. 1, and convincingly showed that iron atom in $FeS_2$ has indeed no magnetic moment associated with it, and the electronic field gradient (efg) and asymmetry parameter were found to be negative and zero respectively. The reported paramagnetic/diamagnetic susceptibilities must be entirely due naturally occuring trace impurities, and the six valence electrons must occupy the three lowest energy levels to give rise to a net spin of zero[4]. As a result there are no unpaired electrons and any efg at the iron nucleus must be due to some other mechanism.

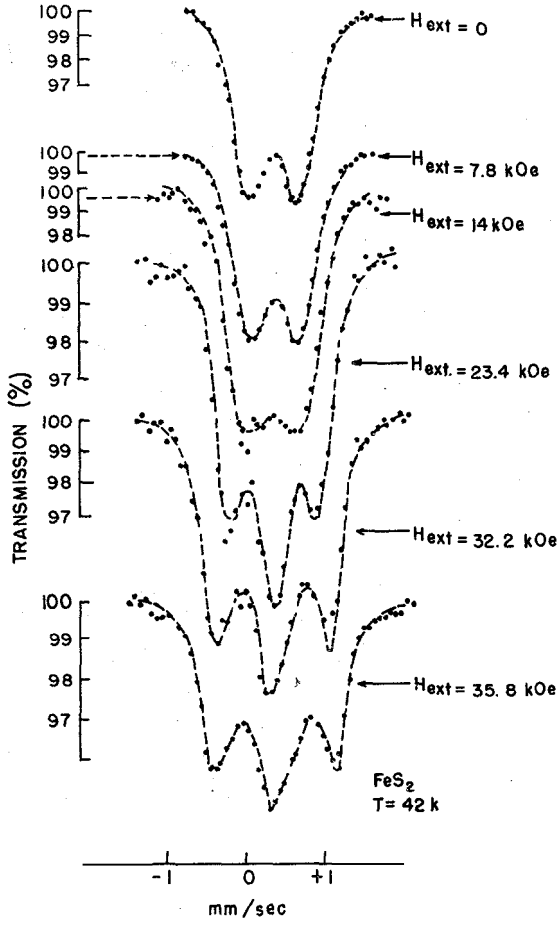


Fig.1 - Mtissbauer spectra of pyrite at 4.2K and in the presence of different external magnetic fields, (after Montano & Seehra, ref.10).

Semiconducting properties are observed for pyrite in which $e^*_g$ levels are expected to overlap to form a band. The observed energy gap and large negative Seebeck coefficient support a conduction process via electrons excited from the localized $t^*_{2g}$ levels into the $e^*_g$ band. Bither *et al.*[11] determined resistivity (1.74 Ohm-cm at 25°C), activation energy (0.20ev at 298K and 0.46 at 500K) and Seebeck coefficient (-500μv/degree ) in pyrite. Natural pyrite exhibits both *n*-and *p*-type semiconduction, sometimes with the same crystal. it has been suggested that natural pyrite formed out at lower temperatures tends to be *p*-type (iron deficient) whereas high temperature pyrite tends to be *n*-type (sulphur deficient). Electron mobility in pyrite is highly variable[12] but generally is about two orders of magnitude greater than hole mobility[13]. Marcasite also exhibits a similar range of electrical and magnetic properties[12].

Mössbauer studies have been reported by many workers. Solomon[14], Imbert *et al.*[15], showed the simple quadrupole interaction for pyrite and marcasite. Kerler and coworkers[16] reported that the isomer shift of pyrite is characteristic of the valency bond of Fe(II) compounds. The quadrupole splitting and the temperature dependence of Q.S. in $FeS_2$ compounds are also not uncharacteristic of Fe(II) compounds. Temperley and Lefvre[7] and Morice *et al.*[17] studied pyrite and marcasite at 300K and 81K and reported isomer shift and quadrupole splitting. Goodman and Richardson[18,19] used on line computer for Mössbauer experiments for three orientations (111, 100 and 110 planes) of pyrite to predict the |111| axis as the principal electric field gradient axis. The effect of pressure upto 200K bar on Mössbauer parameters in pyrite was reported by Vaughan *et al.*[20,21]. The increase in pressure is accompanied by an appreciable decrease in the isomer shift, fig. 2(a), and was attributed to an increase in s-electron density at the iron nucleus. Pyrite also exhibits a 14% increase in the quadrupole splitting at 200K bar, fig. 2(b). Vaughan & Drickamer[21] attributed this change to variation in electric field gradient arising from both valence electron and lattice site asymmetry, and discussed in terms of ferric ion; but this seems unlikely. The low-spin electronic configuration of $Fe^{2+}(t_{2g}^6)$ in pyrite suggests that the change is due solely to distortion in sites which could itself reduce the degeneracy of the $t_{2g}$ and eg orbitals. Gerard[22] also studied the semimetallic compounds to look into the nature of ligation. Lofelhocz *et al.*[23] and Montano[24] found iron sulphide while studying iron compounds in coal by Mössbauer spectroscopy. Vainshtein *et al.*[25] stu-

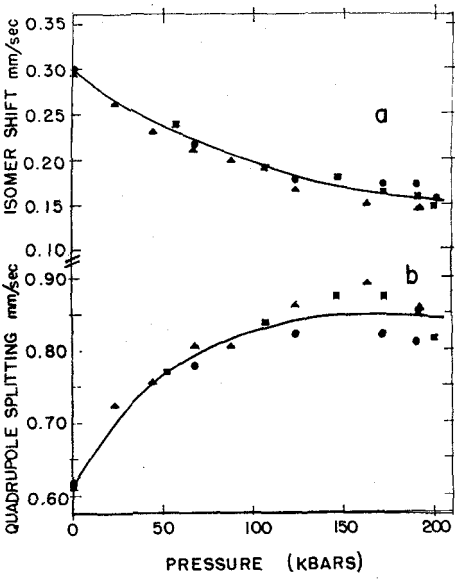


Fig.2 - The effect of pressure on Wssbauer parameters in pyrite (after Vaughan E Drickamer, ref. 21).
(a) Isomer shift vs pressure
(b) Quadrupole splitting vs pressure

died the Mössbauer spectra of iron in pyrite and marcasite of different origins. Zhetbaev and Kaipov[26] also reported Mössbauer parameters of iron sulphide. Goncharov et *al.*[27,28] studied the $FeS_{1+x}$ system (with $x = 0$ to 0.135) and iron sulphide also. The observed change of Mössbauer pararneters was attributed to phase transitions and related to the variation of the concentration of iron vacancies with composition. Baker[29] evaluated the pyritic oxidation. Suzdalev *et al.*[30] studied the anisotropy of the probability of Mössbauer effect in single crystals of pyrite between 90K and 800K. For single crystal pyrite, data agreed with the results of polycrystalline samples. Anisotropy was observed in the iron atom vibrations in $FeS_2$ crystals. Figueiredo *et al.*[31] considered the distortion of nearly 4.3°, in the iron - sulphur octahedra of the unit cell of pyrite, to be responsible for the quadrupole splitting. Phase transformation study in $FeS_2$ during therrnal treatrnent has been reported by Cherkes et *al.*[32]; Abishev *et al.*[33] reported the pyrite therrnal decomposition and showed that the decomposition process has proceeded by formation of alternate composition pyrr-

hotites. Dickson *et al.*[34] studied iron in organic materials from natural sedimentary environments, and in samples of Kerogen obtained a spectra corresponding to the pyrite spectra. Tyulenev *et al.*[35] investigated the cunversion of iron sulphides during grinding.

Kothekar[36] used a molecular orbital approach to the chemical interpretation in $FeS_2$. Burns and Vaughan[37] reported a molecular energy level diagram for pyrite. The tetrahedral coordination of the sulphuratoms to three metals and another sulphur was suggested to be the involvement of 3s and 3*p* orbitals ($sp^3$ hybridized) in forming σ bonds. One hybrid $sp^3$ orbital from each of the six sulphur forms six a bonds with $d^2sp^3$ hybrid orbitals of the central transition metal. The $d^2sp^3$ hybrids consists of the two eg orbitals ($d_{x^2-y^2}$ and $d_{z^2}$), the one 4*s* orbital and the three 4*p*-orbitals. Bither *et al.*[11] assumed that the three $t_{2g}$ orbitals ($d_{xy}$, $d_{yz}$, $d_{xz}$) of the transition metal remain nonbonding. It was also suggested that the paired electrons in the nonbonding $t_{2g}$ orbitals may forrn Π bonds with vacant $t_{2g}$-type 3 orbitals of the sulphur atoms. This would result in the increased energy separation between nonbonding $t_{2g}$ and antibonding e*g levels. But, Kjekshus & Nicholson[38] critically evaluated Mössbauer and bond length data for the pyrite and the marcasite and found no evidence to support Π-backbonding between metal and the non-metal atoms. Overlaping ofmolecular orbitals in an $FeS_2$ crystal causes broadening into bands[11,39]. The main bonding molecular orbitals now form the filled a band and the corresponding antibonding orbitals the empty σ* bond, consisting the main valence and conduction bands respectively. The iron 3*d* orbitals then lie between these in energy, the $t_{2g}$ orbitals being regarded as essentially localized on the cation but the eg orbitals forming a band through overlap via sulphur intermediaries. Thus, conduction in pyrite occurs when electrons are excited into the band formed from e*g orbitals. Finklea, III *et al.*[40] investigated the bonding mechanism in pyrite using Mössbauer effect and X-ray crystallography. Considering the bonding in relation to the origin of the quadrupole splitting and the angular variation of the recoilfree it was found that neither crystal-field effects nor nonstoichiometry are enough to account for the observed splitting. Consideration of molecular orbital effects however showed that a very small amount of electron delocalization is enough to cause the observed splitting because of the strong effects the valence electrons have on the iron nucleus. It was also found that the

recoilfree fraction is practically inifependent of angle. The vsriation of isomer shift with temperature was also reported and was interpreted to mean that vibrational modes corresponding to Raman modes are not excited in the pyrite lattice between 10K and 300K, complementing reported[41] IR spectra which skows no such mode between 190 and 660 $cm^{-1}$ (equivalent to 274 and 950K). Ward and Howard[42] related the quadrupole splitting with electric field gradient at Fe sites calculated on the basis of point charge model for both pyrite and marcasite. Krammer and Klein[43] have determined the relative binding energies of iron $3p$ and sulphur $2p$ electrons in $FeS_2$ which are of interest to correlate directly with atornic charge and present an interesting parallel with isomer shift. Single crystal Mössbauer experiment have been reported by many workers[15,18,30,40,44-47].

## 2. CRYSTAC STRUCTURE AND EXPERIMENTAL

### Crystal Structure: Pyrite

Pyrite occures abundantly with coal deposits in nature as large cubic crystals, with crystal system cubic, space group Pa3, four molecules per unit cell. The metal (Fe) ions are coordinated to six sulphur which are locsted at the centers of a distorted octahedron, fig.3. The sulphur ions are tetrahedrnlly ccordinated to three Fe and another S, with a = = 5.4179 Å, and the iron atoms are located at (0,0,0), (0,1/2,1/2), (1/2, 0,1/2) and (1/2,1/2,0) and the sulphur atoms are located at general positions ± ($U$,$U$,$U$), ($U$+1/2, 1/2-$U$, $\bar{U}$), ($\bar{U}$, $U$+1/2, 1/2-$U$) and (1/2-$U$, $\bar{U}$,$U$+1/2) with $U$ = 0.386 with dumbbell shaped $S_2$ pairs around Fe. The correct positions of sulphur atoms depend on the parômeter U, where $U$ is the atomic coordinate in fractions of the cell size. Finklea, III, *et al.*[40] showed the effect on quadrupole splitting and the asymmetry parameter by varying values of U. The distances and angles of the slightly distortec! octahedron forned by iron and sulphur, fig. 4, are:

| | | |
|---|---|---|
| Fe - S (6) | = | 2.262 ± 0.003Å |
| S - S (1) | = | 2.177 ± 0.004Å |
| S - Fe - S (6+6) | = | 85.57 ± 0.10° |
| | = | 94.43 ± 0.10° |

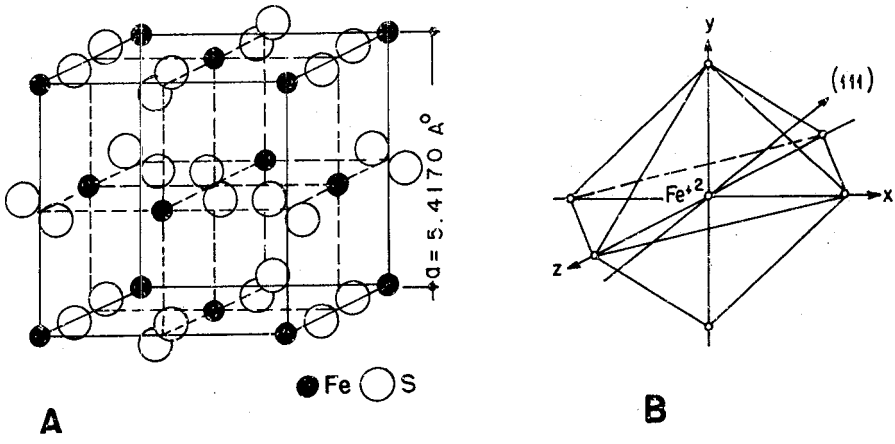


Fig.3 - Structure of pyrite
A) Unit cell
(B) Local surrounding of an iron atom, sulphur atom are found at octahedral sites which are deformed along |111| direction.

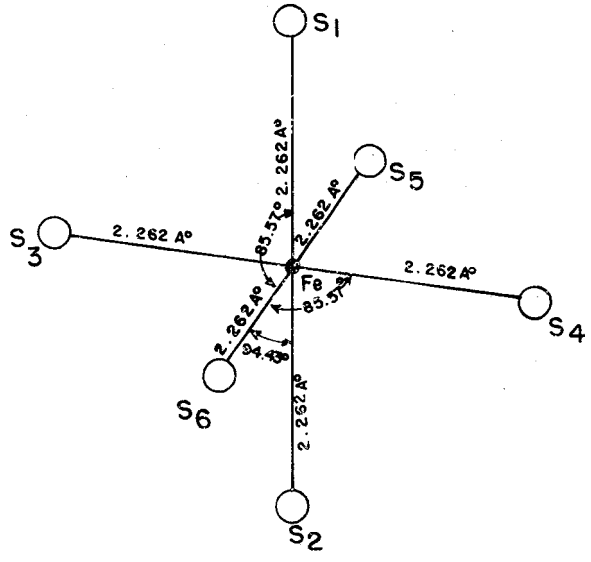


Fig.4 - Schematics of pyrite showing distances between sulphur ions around iron and angles between the octahedral axes.

$$Fe - S - Fe\ (3) = 115.71 \pm 0.12^{0}$$
$$S - S - (Fe\ (3)) = 102.13 \pm 0.13^{0}$$

There are many reports[40,48] on the structure of pyrite.

## Marcasite

There are many reports[49] of the studies of marcasite structure, which is orthorhombic, fig. 5. Most of the available data point to a bi-molecular unit of cell dimensions, $a = 4.436A^0$, $b = 5.414A^0$, and $c=3.381A^0$. However, faint reflections have been described which seem to call for a tetra molecular cell. In our case we have adopted the following arrangement based on $V_h^{12}$ (Pnnm) group.

Fe : $(2a)$ at $(0,0,0)$; $(1/2, 1/2, 1/2)$

S : $(4g)$ at $\pm (U,V,0)$; $(1/2-U, V+1/2, 1/2)$

with $U = 0.200$ and $V = 0.378$

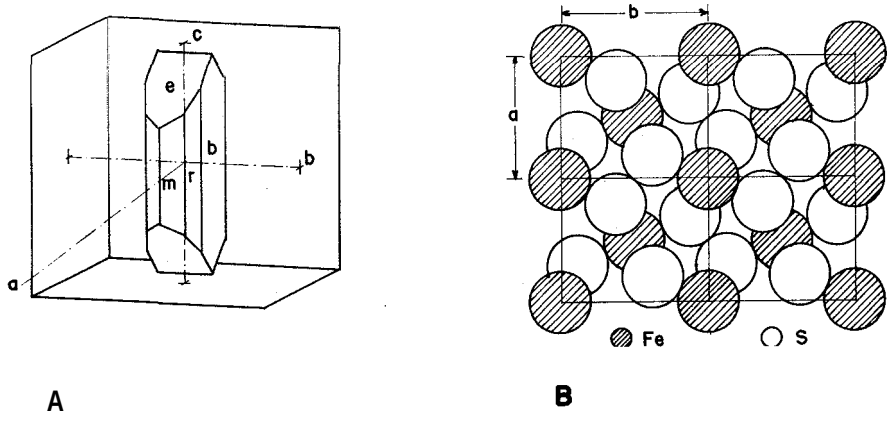


Fig.5 - Structure of marcasite
(A) Defining the orientation relative to crystal axes.
(B) Showing pairs of sulphur atoms with their mid points at the centers of four edges and two faces of the unit cell.

Thus, in this structure which is far from being closed packed, the atomic separations are those of neutral radii. Each iron has three neighbours of Fe - S = 2.2508, and each sulphur has another sulphur at 2.210Å away. The angles and distances of octahedron formed by sulphur around iron are shown in fig. 6.

## Experimental

The Mössbauer spectra were recorded in the standard transmis-

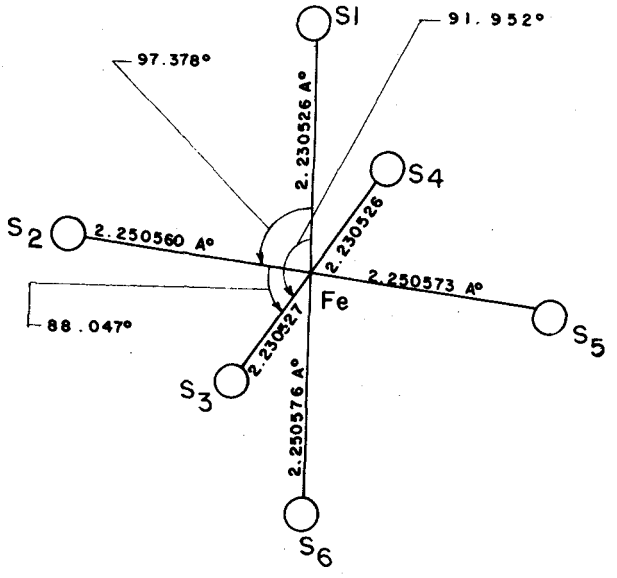


Fig.6 - Schematics of marcasite showing distances between sulphur ions around iron and angles between the octahedral axes.

sion geometry employing a constant acceleration velocity transducer coupled to a source of Co $^{57}$ in Pd matrix with an initial activity of 25mCi/s. A methane-argon filled proportional counter was used for the detection of the Mössbauer transition and a MCA was used to store the spectra. The calibration of the velocity per channel and the linearity verification was done with a (1.9mg $Fe^{57}/cm^2$) iron foil. The pyrite crystals used were 1 $cm^3$, sufficiently large to permit cutting the crystals in the desired directions. However, the marcasite crystals were small (1×1×3 $mm^3$); therefore it was not possible to cut the crystals in all desired directions. The identification of the crystal axes was done morphologically. The crystals were cut and grourid-down. Fig.7 shows the schematics of the absorption of Mössbauer transition by the single crystal absorbers. Typical Mössbauer spectra of pyrite and marcasite are shown in figs. 8A and 8B respectively. Variation of linewidth with absorber thickness in pyrite is depicted in fig. 9. Table 1 shows the values of isomer shift and quadrupole splitting for pyrite and marcasite.

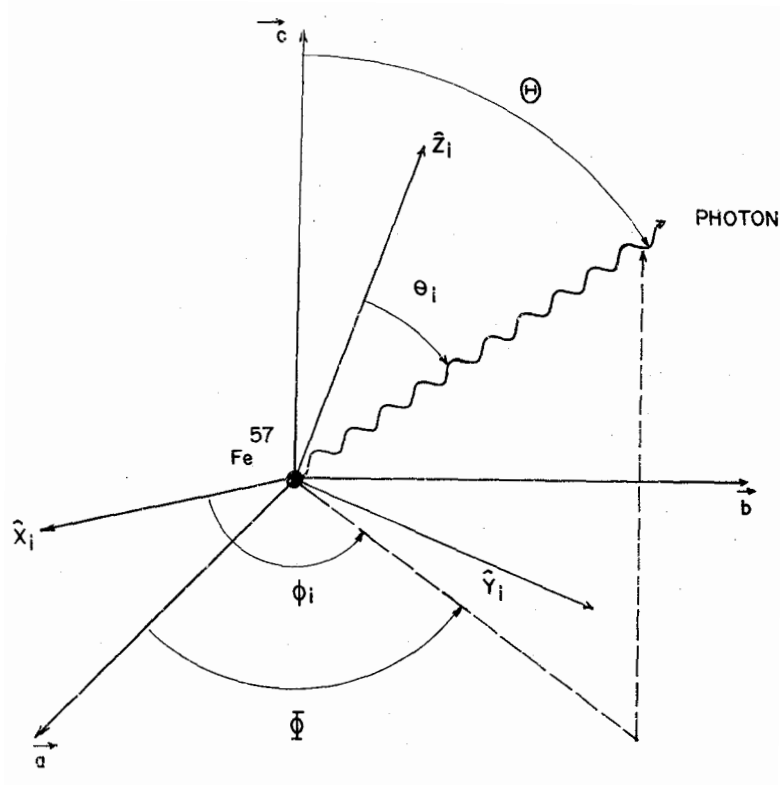


Fig.7 - Schematics of absorption of 14.4kev y-rays by the iron sulphide ($Fe^{57}S_2$) single crystal absorbers.

## 3. THEORY AND ANALYSIS

### Electric Field Gradient

In a quadrupole split spectrurn, let $\alpha_3$ and $\alpha_1$ be defined as the absorption peaks corresponding to $\pm \frac{3}{2} \rightarrow \pm \frac{1}{2}$ and $\pm \frac{1}{2} \rightarrow \pm \frac{1}{2}$ transitions, respectively. Then, for a monochromatic unpolarised source and a single crystal absorber withi equivalent sites per unit cell, the area ratio after Zory[50] is

$$(\alpha_3 \times \alpha_1)^{-1} = \left(\left(\sum_{\text{sites}} p_3(\theta_i,\phi_i) f'(\theta_i,\phi_i)\right) \times \left(\sum_{\text{sites}} p_1(\theta_i,\phi_i) f'(\theta_i,\phi_i)\right)^{-1}\right) \qquad (1)$$

where $p_3(\theta_i,\phi_i)$ and $p_1(\theta_i,\phi_i)$ are the relative angular dependent absorption probabilities for the transition ± 3/2 → ± 1/2 and ± 1/2 → ± 1/2 respecti-

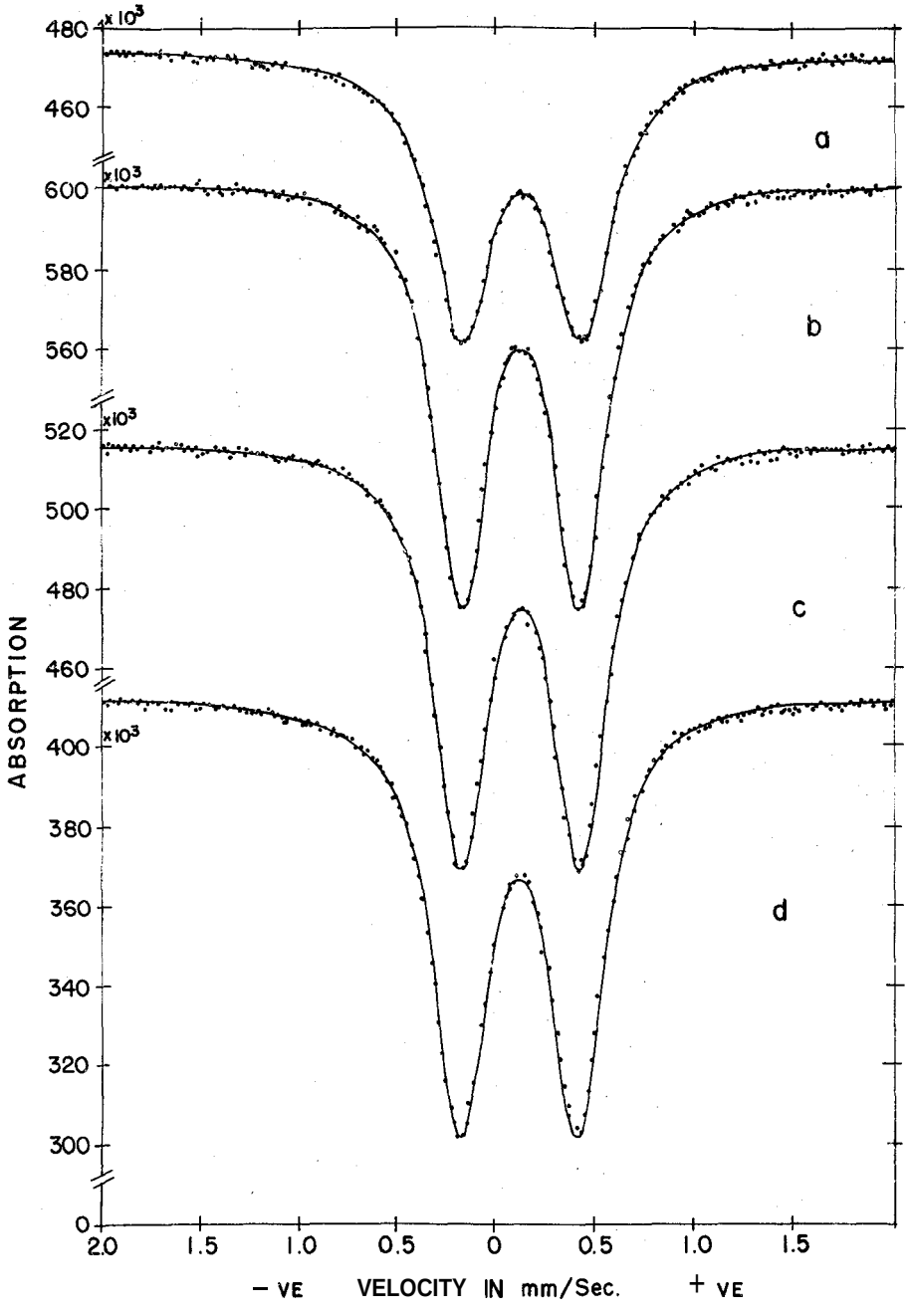


Fig.8A - Mössbauer absorption spectra of pyrite
(a) polycrystalline, and monocrystalline (b) 111 plane (c) 110 plane and (d) 100 plane.

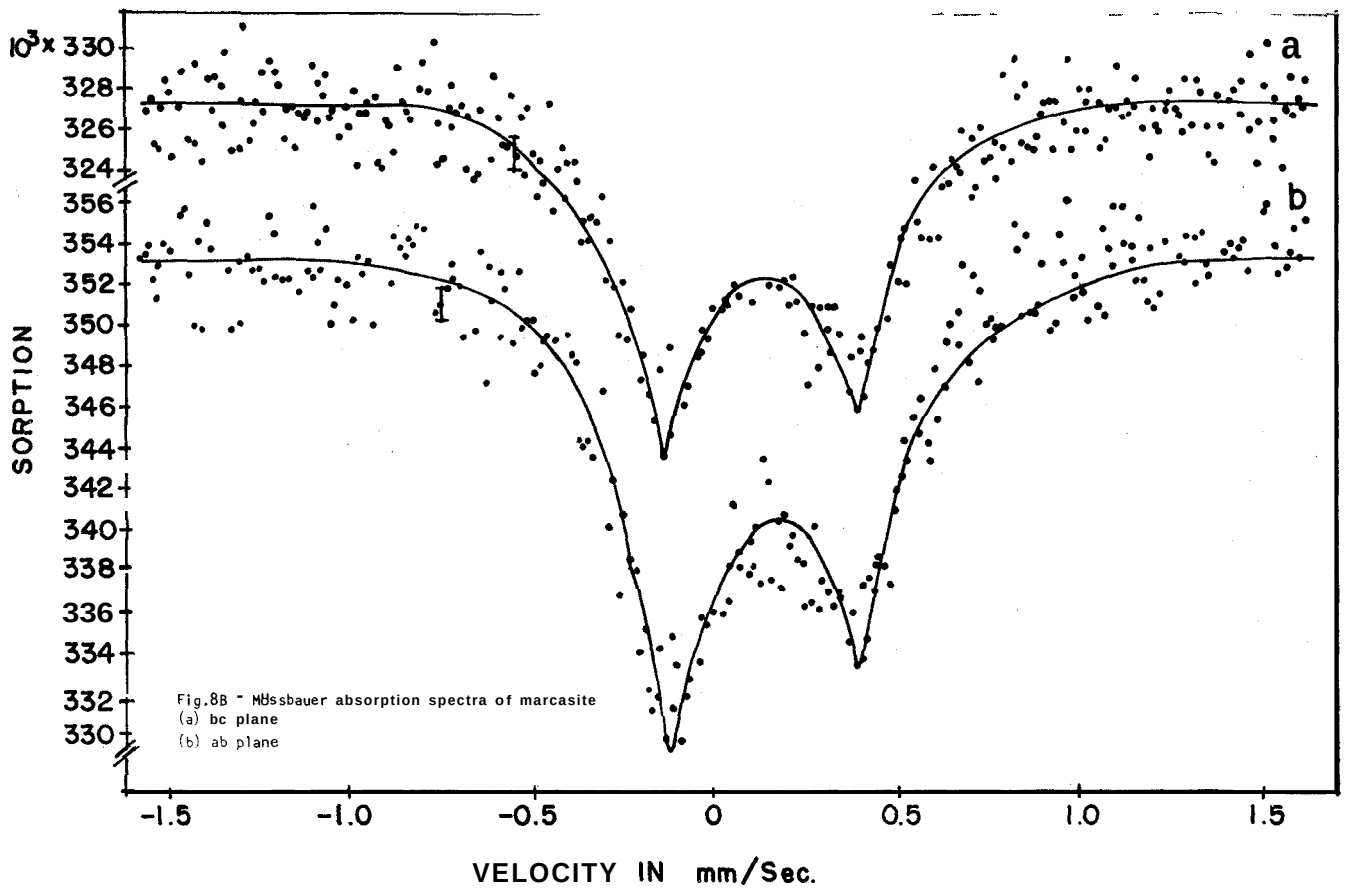


Fig.8B - Mössbauer absorption spectra of marcasite
(a) bc plane
(b) ab plane

| Absorber | Absorber temperature in $^0K$ | Isomershift (Fe) in mm/sec. | Quadrupole splitting in mm/sec. | Reference |
|---|---|---|---|---|
| $FeS_2$ | | | | |
| (pyrite) | 300 | 0.314(2) | 0.614(6) | 7 |
| | 81 | 0.407(3) | 0.620(9) | |
| | 300 | 0.23 | 0.77 | 21 |
| | (50Kbar) | | | |
| | 297 | 0.25(1) | 0.62(1) | 10 |
| | 78 | 0.36(1) | 0.64(1) | |
| | 4.2 | 0.43(1) | 0.66(1) | |
| | RT(300) | 0.325(5) | 0.62(2) | 44 |
| | | 0.325(5) | 0.62(1) | 46 |
| | | 0.316(5) | 0.616(2) | 31 |
| | 77 | 0.409(5) | 0.626(2) | 31 |
| | 296 | 0.33(1) | 0.615(6) | 42 |
| $FeS_2$ | | | | |
| (marcasite) | 300 | 0.277(2) | 0.506(7) | 7 |
| | 81 | 0.373(2) | 0.504(6) | |
| | 300 | 0.277(5) | 0.506(5) | 45 |
| | RT | 0.29(1) | 0.50(1) | 17 |
| | RT | 0.23 | 0.52 | 28 |

Table 1. Values of isomershift (with respect to iron) and quadrupole-splitting for pyrit- and marcasite.

vely; $f'(\theta_i,\phi_i)$ is the Lamb-Mössbauer fraction. The angles $(\theta_i,\phi_i)$ define the incident $\gamma$-ray beam with respect to the electric field gradient axes $(\hat{X}_i, \hat{Y}_i, \hat{Z}_i)$ and $a,b,c$ are the mutually orthogonal axes, fig.7. Employing the explicit expressions for $p_3$ and $p_1$, expressing the angles $(\theta_i,\phi_i)$ in terms of known experimental angles and relating a site $i$ to the crystal axes $(a,b,c)$ the area ratios are

$$a_3/a_1 = \left\{\sum_i f'(\theta_i,\phi_i)\left\{4\left[\frac{3+\eta^2}{3}\right]^{1/2} + \left[3\cos^2\theta_i - 1 + \eta\sin^2\theta_i\cos 2\phi_i\right]\right\}\right\}$$
$$\left\{\sum_i f'(\theta_i,\phi_i)\left\{4\left[\frac{3+\eta^2}{3}\right]^{1/2} - \left[3\cos^2\theta_i - 1 + \eta\sin^2\theta_i\cos 2\phi_i\right]\right\}\right\} \quad (2)$$

and $\cos\theta_i$ is related to the experimental angles $(\Theta,\Phi)$

$$\cos\theta_i = \sin\Theta.\cos\Phi\ (\hat{Z}_i.a) + \sin\Theta.\sin\Phi\ (\hat{Z}_i.b) + \cos\Theta\ (\hat{Z}_i.c) \quad (3)$$

Here $(\hat{Z}_i.a)$, $(\hat{Z}_i.b)$ and $(\hat{Z}_i.c)$ are the cosines of the angles between efg $\hat{Z}$ axis and the crystallographic axes.

## Marcasite

The area ratios calculated from equation (2), assuming different Fe-S axes to be the axes of efg, are tabulated in table 2. The calculated area ratios assuming we know the axes of the efg agree with the experimental value. $Fe\text{-}S_6$ is the direction of $\hat{Z}$ axis of the efg where as $Fe\text{-}S_2$ and $Fe\text{-}S_3$ are $\hat{X}$ and $\hat{Y}$ axes, respectively. The direction cosines of $(\hat{X}, \hat{Y}, \hat{Z})$ axes with respect to the $(a,b,c)$ axes are given in table 3.

Since the area ratio of the lower velocity to the higher velocity peaks is $a_3/a_1$ and not $a_1/a_3$, it follows that the quadrupole interaction $eq$ is negative, and this finding is in agreement with Donaldson et al.[51], who carried out Mössbauer experiments with $Sb^{121}$ on compounds with marcasite structure and reported that $V_{zz}$ is negative in all cases.

The asymmetry parameter is zero.

## Pyrite

The area ratios calculated from equation (2) are tabulated in table 4A. The calculated values of area ratio $(a_3/a_1)$, assuming that the crystallographic axes are the axes of efg, do not agree[44] with the experimental value, table 4B, of 1.00 + 0.02 which is independent of the crystal orientation.

| Absorber orientation Θ | Φ | Fe-$S_6$ axis direction as $\hat{Z}$ axis of efg | Fe-$S_3$ axis direction as $\hat{Z}$ axis of efg | Fe-$S_5$ axis direction as $\hat{Z}$ axis of efg | Experimental Peak Area ratio | Linewidth mm/sec. | Absorber thickness mm | Reference |
|---|---|---|---|---|---|---|---|---|
| 0 | 0 | 0.69 | 0.68 | 2.17 | | | <0.2 | 45 |
| $\frac{\pi}{2}$ | 0 | 1.24 | 1.02 | 0.76 | 1.20 | 0.304(6) | <0.2 | 45 |
| $\frac{\pi}{2}$ | $\frac{\pi}{2}$ | 1.16 | 1.42 | 0.60 | 1.15 | 0.298(6) | <0.2 | 45 |

Table 2. Experimental and calculated peak area ratio for different orientations with $\eta$=0 for marcasite, calculated on the basis of equation (2).

| | |
|---|---|
| $X_a$ | 0.5915 |
| $X_b$ | 0.2936 |
| $X_c$ | 0.7513 |
| $Y_a$ | 0.3943 |
| $Y_b$ | 0.9096 |
| $Y_c$ | 0.0 |
| $Z_a$ | 0.6896 |
| $Z_b$ | 0.2989 |
| $Z_c$ | 0.6597 |

Table 3. Direction cosines of efg with respect to the crystal axes (a, $b$, c) for marcasite.

| Absorber orientation $\Theta$ | $\Phi$ | Fe-$S_1$ axis direction as $\hat{Z}$ axis of efg | Fe-$S_3$ axis direction as $\hat{Z}$ axis of efg | Fe-$S_5$ axis direction as $\hat{Z}$ axis of efg |
|---|---|---|---|---|
| 0 | 0 | 2.27 | 0.674 | 0.674 |
| $\frac{\pi}{2}$ | 0 | 0.674 | 0.674 | 2.27 |
| $\frac{\pi}{2}$ | $\frac{\pi}{2}$ | 0.674 | 2.27 | 0.67 |
| $\frac{\pi}{2}$ | $\frac{\pi}{4}$ | 0.60 | 1.79 | 0.832 |
| $\frac{\pi}{2}$ | $-\frac{\pi}{2}$ | 0.756 | 0.832 | 1.799 |
| $\frac{\pi}{4}$ | $\frac{\pi}{2}$ | 1.799 | 0.832 | 0.60 |
| $\frac{\pi}{4}$ | 0 | 0.832 | 0.60 | 1.799 |

Table 4A. Peak area ratios for different orientations with $\eta = 0$ for pyrite, calculated on the basis of equation (2).

| Absorber | Experimental peak area ratio | Thickness of absorber in mm | linewidth mm/sec. | Reference |
|---|---|---|---|---|
| Powder | 0.97 | | | 15 |
| 100 plane | 0.86 | | | 18 |
| 100 | 1.33 | | | 18 |
| 100 | 0.89(2) | <0.2 | 0.30(1) | 44 |
| O10 | 0.89(2) | <0.2 | 0.30(1) | |
| 001 | 1.00(2) | <0.2 | 0.30(1) | |
| Powder | 1.00(2) | <0.2 | 0.30(1) | |
| 100 | 1.03(1) | 100-200μ | | 30 |
| 110 | 1.03(1) | | | |
| Powder | 1.03(1) | | | |
| 100 | 1.000(16) | | | 40 |
| 010 | 1.004(11) | | | |
| 110 | 1.008(20) | | | |
| Powder | 1.013(31) | | | |
| Powder | 1.0 1(2) | 0.165 | 0.377 | 46 |
| 111 | 1.00(2) | 0.06 | 0.298 | |
| 110 | 1.00(2) | 0.07 | 0. 328 | |
| 100 | 1.02(2) | 0.05 | 0.318 | |

Table 4B. Experimental peak area ratio, thickness of absorber and linewidth of pyrite.

With point charge model, the efg tensor of pyrite is ofthe following form[44],

$$V_{ij} = (1-\gamma_\infty)\begin{vmatrix} 0 & A & A \\ A & 0 & A \\ A & A & 0 \end{vmatrix} \qquad (3)$$

where

$$A = -\,6q_{eff}(V-1/2)^2/(3U^2-2U+1/2)^{5/2} \qquad (4)$$

$$= +\ 0.03824\ (A^0 - 3/e) \qquad (5)$$

when only the first neigbours with effective charge, $q_{eff}$ = -2e and the

crystallographic axes as the coordinate axes are taken into considerction. Taking the crystal symmetry into considerations, the efg tensors for the iron sites (0,0,0), (1/2,1/2,0), (1/2,0,1/2) and (0,1/2,1/2) are respectively

$$(1-\gamma_\infty)\begin{vmatrix} 0 & A & A \\ A & 0 & A \\ A & A & 0 \end{vmatrix}, \quad (1-\gamma_\infty)\begin{vmatrix} 0 & -A & -A \\ -A & 0 & A \\ -A & A & 0 \end{vmatrix}, \quad (1-\gamma_\infty)\begin{vmatrix} 0 & A & -A \\ A & 0 & -A \\ -A & -A & 0 \end{vmatrix} \quad \text{and} \quad (1-\gamma_\infty)\begin{vmatrix} 0 & -A & A \\ -A & 0 & -A \\ A & -A & 0 \end{vmatrix} \tag{6}$$

However, by convention, we define

$$|V_{zz}| \geq |V_{yy}| \geq |V_{xx}| \tag{7}$$

thus

$$V_{zz} = 2A(1-\gamma_\infty) \tag{8}$$

and

$$V_{yy} = V_{xx} = -A(1-\gamma_\infty) \tag{9}$$

$$\eta = \frac{V_{xx} - V_{yy}}{V_{zz}} = 0 \tag{10}$$

Thus $\hat{Z}$ axes are $|1,1,1|$ , $|-1,1,1|$ , $|1,1,-1|$ and $|1, -1, 1|$ respectively, (for different sites of iron) and make an angle of $\cos^{-1}1/\sqrt{3}$ with the crystallographic axis; and X and Y axes remain undetermined.

On simplyfyiny equation (2) we obtain

$$a_3/a_1 = \frac{3(1+\cos^2\theta_i)}{5-3\cos^2\theta_i}$$

since the area ratio, $a_3/a_1$, is unity, $\theta = \cos^{-1} 1/\sqrt{3}$ , and is in accord with the simple point charge model. Although the four sites of iron are equivalent, the fact that the crystal structure is of cubic symmetry requires that the efg must either vanish at the iron sites, which is contrary to the experimental fact of $AE_Q$ = 0.62 mm/sec, or that the efg principal axes must be oriented in such a way that the average effects summed over the four sites must satisfy the given symmetry.

## Mean Square Displacement

The recoilfree fraction is given by

$$f_i = e^{-K^2\langle r^2\rangle}$$

Now, let $\langle x^2\rangle$, $\langle y^2\rangle$ and $\langle z^2\rangle$ represent the three components of the diagonaised MSD tensor. Then in any direction $\hat{K}$, $\langle r^2\rangle$ is[52]

$$\langle r^2\rangle_i = \langle x^2\rangle \sin^2\delta \cos\varepsilon + \langle y^2\rangle \sin^2\delta \sin^2\varepsilon + \langle z^2\rangle \cos^2\delta$$

here $\delta$ and $\varepsilon$ are the polar and azimuthal angles of $\hat{K}$. If, a , $\beta$ and $\gamma$ are the Euler's angles specifying the orientation of MSD principal axes with respect to the crystallographic axes, then the MSD along a, $b$, and c are

$$\langle r_a^2\rangle = \langle x^2\rangle (\cos\alpha\cos\gamma - \sin\alpha\cos\beta\sin\gamma)^2 + \langle y^2\rangle (\cos\alpha\sin\gamma - \sin\alpha\cos\beta\cos\gamma)^2 c + \langle z^2\rangle (\sin^2\alpha \sin^2\beta) \quad (11)$$

$$\langle r_b^2\rangle = \langle x^2\rangle (\sin a\cos\gamma + \cos a\cos\beta\sin\gamma)^2 + \langle y^2\rangle (\sin\alpha\sin\gamma - \cos a\cos\beta\cos\gamma)^2 + \langle z^2\rangle (\cos^2\alpha \sin^2\beta) \quad (12)$$

$$\langle r_c^2\rangle = \langle x^2\rangle \sin^2\beta \sin^2\gamma + \langle y^2\rangle \sin^2\beta \cos^2\gamma + \langle z^2\rangle \cos^2\beta \quad (13)$$

However in pyrite the efg axis is a symmetry axis, (and $a = b = c$)

$$\langle r_a^2\rangle = \langle r_b^2\rangle = \langle r_c^2\rangle \quad (14)$$

The above equations (11), (12) and (13) can be solved with three restrictions:

1. $\langle x^2\rangle \neq \langle y^2\rangle \# \langle z^2\rangle$, in this case no further solution is possible.
2. $\langle x^2\rangle = \langle y^2\rangle = \langle z^2\rangle$, is an abvious case in pyrite, but a more general solution than this solution will be
3. $\langle x^2\rangle = \langle y^2\rangle \neq \langle z^2\rangle$

Putting the restriction 3 in equations (11), (12) and (13), we obtain

Thus, for each site of iron, efg and MSD can be considered to coincide with each other.

After Bancroft[53], the experimental linewidth is

$$\Gamma_{exp} = \Gamma_a + \Gamma_s + 0.27\ \Gamma_H X,$$

where $\Gamma_a + \Gamma_s$ is the width $\Gamma_{exp.}$ extrapolated to $X = 0$, $\Gamma_H$ is the natural linewidth; and $X = nf\sigma_0$, here n is the number ot atoms of Mössbauer isotope/cm$^2$, $f$ is the Mössbauer fraction and $\sigma_0$ is the maximum cross-section at resonance and is[54] $255.754\times10^{-20}$ cm$^2$. With the relation of pyrite absorber thickness and linewidth, fig.9, we determine the value of Mössbauer fraction to be $0.202\pm0.020$ at room temperature; and using the value of $K^2 = 5.334\times10^{17}$ from MEDI[55], we obtain $\langle x^2\rangle = 0.434\times10^{-18} \pm 0.023$ cm$^2$ at room temperature.

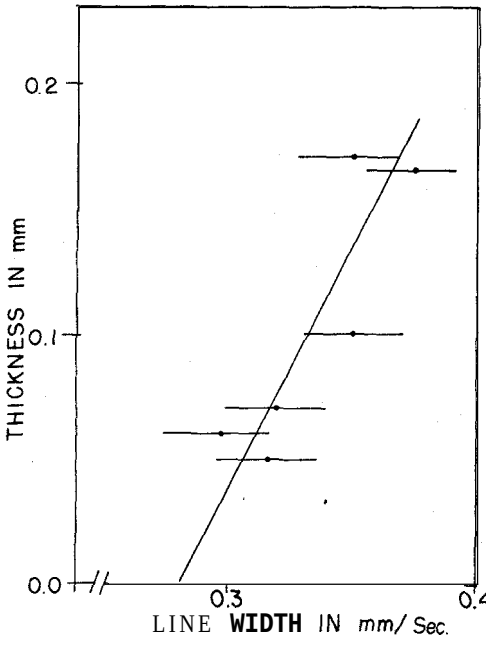


Fig.9 - Linewidth variation with absorber thickness (pyrite).

Suzdalev *et al.*[30] and Finklea, III, *et al.*[40] have also calculated the magnitude of the principal axes of the mean squared displacement of the Fe atonis, i.e. $\langle x^2 \rangle$ parallel and perpendicular to |111| axis, Suzdalev *et al.* found the difference in magnitude of the principal axis by about a factor of two while Finklea, III, *et al.* found that the difference between the two values cannot be greater than 9%.

## Area Ratio Unity Independent of Orientation

It is interesting to note that the experimental peak area ratios in pyrite, table 4B, are equal to unity, independent of orientation (except for the first five measurements reported, which most likely are due to interferring impurities).

For the thin absorber limit the peak area ratio given in equation (2) and a relation of cos $\theta_i$ is in equation (3), but $f_i = e^{-K^2\langle x^2 \rangle}$ for $\langle x^2 \rangle = \langle y^2 \rangle$

$$f_i = e^{\{-K^2 |\langle x^2 \rangle \sin^2\theta_i + \langle z^2 \rangle \cos^2\theta_i|\}}$$

Now putting the values of $\cos^2\theta_i$ for each site of iron, table 5, the following peak area ratios are given:

$$a_i \sim \exp\left| -\frac{K^2}{3}(2\langle x^2 \rangle + \langle z^2 \rangle)\right| \{(4 \pm A_+)\, e^{-\frac{K^2}{3}\nu A_+} + (4 \pm B_+)\, e^{\frac{K^2}{3}\nu B_+} + (4 \pm A_-)\, e^{-\frac{K^2}{3}\nu A_-} + (4 \pm B_-)\, e^{\frac{K^2}{3}\nu B_-}\} \qquad (15)$$

where $\nu = \langle z^2 \rangle - \langle x^2 \rangle$ and

$$A_\pm = \sin^2\theta \sin 2\phi \pm \sin 2\theta (\cos\phi + \sin\phi)$$

$$B_\pm = \sin^2\theta \sin 2\phi \pm \sin 2\theta (\cos\phi - \sin\phi)$$

the upper and lower sign of $\pm$ in $a_i$ represent $a_3$ and $a_1$ respectively. Now, if in equation (15) $\nu$ is zero, which means that the recoilless fraction is isotropic, then the area ratio will always be unity for any values of $\theta$ and $\phi$ in case of a monocrystalline pyrite sample. In other words area ratio of unity will be independent of orientation of the crystal with res-

| Fe site | Direction of efg $\hat{Z}$-axis | $\cos^2\theta_i$ |
|---|---|---|
| (0 0 0) | \| 1,1,1\| | $\frac{1}{3}\left[1+\sin^2\theta\sin^2\Phi + \sin^2\theta(\cos\Phi + \sin\Phi)\right]$ |
| $(\frac{1}{2}\ \frac{1}{2}\ 0)$ | \|-1,1,1\| | $\frac{1}{3}\left[1-\sin^2\theta\sin^2\Phi + \sin^2\theta(-\cos\Phi+ \sin\Phi)\right]$ |
| $(\frac{1}{2}\ 0\ \frac{1}{2})$ | \|1,1,-1\| | $\frac{1}{3}\left[1+\sin^2\theta\sin^2\Phi - \sin^2\theta(\cos\Phi + \sin\Phi)\right]$ |
| $(0\ \frac{1}{2}\ \frac{1}{2})$ | \|1,-1,1\| | $\frac{1}{3}\left[1-\sin^2\theta\sin^2\Phi + \sin^2\theta(\cos\Phi - \sin\Phi)\right]$ |

Table 5. Expression for $\cos^2\theta_i$ ($\theta_i$ being the angle between the y-ray direction and the efg $\hat{Z}$ axis) in terms of experimental angles O and $\Phi$.

pect to the y-ray beam. However, in case of polycrystalline pyrite absorber the area ratio will still be unity because the angular-dependent parts cancel out and the lattice vibrational anisotropy is zero.

## 4. STRUCTURE TRANSFORMATION

Pyrite is the most stable of the disulphides and its thermal stability is upto 742$^0$C. Fleet[56], using the single X-ray technique, studied the phase relationship wnen one mineral inverts to the other (marcasite $\rightleftarrows$ pyrite). Experimentally it is possible to transform pyrite to marcasite and vice versa by varying the external conditions of temperatiire and pressure, perhaps through some transitional form[57], such as $\alpha$-$NiAs_2$. A hypothetical mechanism for the transforrnation frorn the pyrite ta the marcasite type of structure has been suggested by Brostigen & Kjekshus[58] on the basis of postulated reorientation of half of the non-metal pairs in the pyrite lattice. It is simply suggested that for structural transformation to take place ($p \leftrightarrows m$), the |111| axis of pyrite nust go into the b axis of marcasite (efg axes of p and $m$ respectively) or vice versa by undergoing a change of angle of $\cos^{-1} 1/\sqrt{3}$.

## REFERENCES


1. L.Pauling and M.L.Haggins, Z. Kristalliogr. 87, 205 (1934).
2. H.Haraldsen and W.Klemm, Z.Anorg.Alleg.Chem. 223, 409 (1935).
3. H.Haraldsen, Avh. Ncr. Vidensk.-Akad. Oslo. Mat. Naturvidensk Kl, 4.3 (1947).
4. A.Serres, J. Phys. Radium *14*, 689 (1953).
5. L.Pauling in The Nature of Chemical Bond (Cornell U.P.) 1960.
6. F.Hulliger and F.Moorer, J.Phys.Chem.Solids *26*, 429 (1965).
7. A.A.Temperlay and H.W.Lafevre, J.Phys.Chem.Solids 27, 85 (1966).
8. S.Miyahara and T.Teranishi, J.Appl.Phys. *39*, 896 (1968).
9. K.Adachi, K.Sato and M.Takeda, J.Phys.Soc.Japan *26*, 631 (1969).
10. P.A.Montano and M.S.Seehra, Solid State Commun. *20*, 897 (1976).
11. T.A.Bither, R.J.Bouchand, W.H.Cloud, P.C.Donohue and W. J. Siemons, Inorg.Chem. 7, 2208 (1968).
12. T.M.Baleshta and H.P.Dibbs, Mines Branch Technical Bulletin TB 106, (1969) Ottawa, Canada.
13. R.T.Shuey in Semiconducting Ore Minerals Developments In Economic Geology No. 4, (1975). Elsevier, Amsterdam, Holland.
14. I.Soloman, Compt. Rend. *250*, 3828 (1960) ; Compt. Rend. *251*, 2675(1960).
15. P.Imbert, A.Gerard and M.Winterberge , Compt.Rend. *256*, 4391 (1963).
16. W.Kerler, W.Neuwirth, E.Fluck, P.Kuhn and B.Zimmermann, Z.Phys. *173*, 321 (1963).
17. J.A.Morice, L.V.C. Rees and D.T.Rickard, J.Inorg. Nucl. Chem.*31*, 3797 (1969).
18. R.H.Goodman and J.E.Richardson, Rev.Sci.Instrum.*37*, 283 (1966).
19. R.H.Goodman, Chem. Cad. *18*, 31 (1966).
20. P.Debrunner, R.W.Vaughan, A.R.Champion, J.Cohen, J.A. Moyzis Jr., and H.G.Drickamer, Rev. Sci. Instrum. 37, 1310 (1966).
21. R.W.Vaughan and H.G.Drickamer, J.Chem.Phys. 47, 468 (1967).
22. A.Gerard, Coll. Int. Centre Nat. Rech. Sci., No. 157 Orsay (1965) Editions du ceiitre National de la Recherche Scientifiques, Paris, (1967) pp. 55-67.
23. J.F.Lofelhocz, R.A.Friedel and T.P.Kohman, Geochim. Cosmochim. Acta *31*, 2261 (1967).
24. P.A.Montano, Fuel *56*, 397 (1977).

25. E.Ye. Vainshtein, P.M.Valor, G.P.Barasanov and M.Ye. Yakovleva, Geochim. Int. 717 (1967).
26. A.H.Zhetbaev and D.K.Kaipov, Izv. Nauk. Kaz. SSR, Ser. Fiz. Mat. 6, 78 (1968).
27. G.N.Goncharov, Yu.M. Ostanevich, S.B.Tomilov, and L.Cser, Phys. Stat. Solidi 37, 141 (1970).
28. G.N.Goncharov, Yu. M.Ostaneich and S.B.Tomilov, Izv. Akad. Nauk. SSSR, Ser. Geol. 8, 79 (1970).
29. R.A.Baker, Water Res. 6, 9 (1972).
30. I.P.Suzdalev, I.A.Vinogradov and V.K.Imshennik, Sov.Phys. Solid State *14*, 1136 (1972).
31. J.O.Figueiredo and V.K.Garg, Radiochem. Radioanal. Letts. *18*, 233 (1974).
32. I.D.Cherkes and V.P.Shumeyko in Proceedingsof Int. Nat. Conf. On Mössbauer Spectroscopy, Carcow, Poland, Vol.*1*, pp.389 (1975), Eds. A. Z. Hrynkiewicz and J.A.Sawcki. (Wykonano W Powielarni Akademii Górniczo- Hutniczej in S. Staszcca, Carcow, Poland 1975).
33. D.N.Abishev, Yu. B.Voitkovskii, A.V.Astakhov, Z.N.Baltinova and L. J. Sergazina in Proceedins of Int. Nat. Conf. On Mössbauer Spectroscopy, Bucharest, Romania, Vol. *1*, pp 373 (1977), Eds. D.Barb and D.Tarina (Revue Roumaine de Physique and Documentation office, Central Institute of Physics, Bucharest, Romania, 1977).
34. D.P.E.Dickson, L.Heller-Kallai and I.Rozenson, Geochim. Cosmichim.Acta. 43, 1449 (1979).
35. G.V.Tyulenev, G.I.Marks, A.F.Krethman and V.A.Vamek, Inv.Sib.Otd.Akad, Nauk. SSSR. Ser. Khim. Nauk. 14, 21 (1976).
36. V.Kothekar, Procd. Int. Nat. Sci. Acad. Part A, 40, 112 (1974).
37. R.G.Burns and J.D.Vaughan, Am.Mineral. *55*, 1576 (1970).
38. A.Kjekshus and D.G.Nicholson, Acta Chem. Scand. 25, 866 (1971).
39. J.B.Goodenough, J. Solid State Chem. *5*, 144 (1972).
40. S.L.Finklea, III, L. Cathey and E.L.Amma, Acta Crystallogr. Sect. A, 32, 529 (1976).
41. H.H.Eysel, H.Siebert and G.Agiorgitis, Z.Naturforch (B), 24, 932 (1969).
42. J.B.Ward and D.G.Howard, J.Appl. Phys. 47, 388 (1976).
43. L.N.Kramer and M.P.Klein, J.Chem.Phys. 51, 3618 (1969).
44. V.K.Garg, Y.S.Liu and S.P.Puri, J.Appl.Phys. 45, 70 (1974).
45. R.Garg and V.K.Garg, Appl. Phys. 16, 175 (1978).

46. R.Garg, Vishwamitter, V.P.Gupta and V.K.Garg, in Proceedings of Int. Conf. Mössbauer Spectroscopy, 10-14 September 1979, Portoroz, Yugoslavia, J.Phys. C-1, 355 (1980).

47. Y.S.Liu, J.Phys. C-2, 400 (1979); Phys. Rev. *B20*, 71 (1979); T.W.Guettinger and D.L.Williamson, Phys. Rev. *B20*, 3938 (1979).

48. H.Strung, Mineralogical Tablen (Akademie Verlag, Leipzig, 1957); G. Brostigen and A.Kjekshus, Acta Cem. Scand. 23, 2186 (1969) and references therein; E.K.Li, K.H.Johnson, D.E.Eastman and J.L.Freeouf, Phys.Rev.Letts. 32, 470 (1974).

49. M.L.Huggins, Phys. Rev. 19, 369 (1922); Z.Krist. 96, 384 (1937); W. F. de Jong, Physica 6, 325 (1926); J.Garrido, Bull. Soc. Franc. Mineral, 74, 397 (1951); R.W.G.Wycoff, Crystal Structures *1*, 355 (1963); W. Gorzkowski, Acta Physics Polon. 24, 527 (1964); H.Strung, Neus Jahrb. Mineral.Monatsh. 9, 247 (1965); W.B.Pearson, Z.Krist. 121, 449 (1965); G.Brostigen,A.Kjekshus and Chr.Romming, Acta Chem. Scand. 27, 2791 (1973) and references therein; B.Mason, L. G.Berry, in Elements of Mineralogy (W.H .Freeman and Company, San Francisco, 1960) p. 260.

50. P.Zory, Phys. Rev. 140, A1401 (1965).

51. J.D.Donaldson, A.Kjekshus, D.G.Nicholson and M.J.Trecker, Acta Chem. Scand. 26, 3215 (1972).

52. R.W.Grant, R.M.Housley and U.Gonser, Phys. Rev. 178, 523 (1969).

53. G.M.Bancroft in Mössbauer Spectroscopy: An Introduction for Chemists and Geochemists, John Wiley & Sons, New York, USA.

54. Mössbauer Effect Data Index (1976) Ed. J.G.Stevens and V.E. Stevens, Plenum Press, New York, USA (1978).

55. Müssbauer Effect Data Index (1958-1965) Ed. A.H.Muir, Jr., K.J. Ando and H.M.Coogan, Interscience, New York, USA (1966).

56. M.E. Fleet, Can. Mineral 10, 225 (1970).

57. W.N.Stassen and R.D.Heyding, Can.J.Chem. 46, 2159 (1968).

58. G.Brostigen and A.Kjekshus, Acta Chem. Scand. 24, 2983 (1970).